

## Review

# Indocyanine green-incorporating nanoparticles for cancer theranostics

Haolu Wang<sup>1</sup>, Xinxing Li<sup>2</sup>, Brian Wan-Chi Tse<sup>3</sup>, Haotian Yang<sup>1,4</sup>, Camilla A. Thorling<sup>1</sup>, Yuxin Liu<sup>5</sup>, Margaux Touraud<sup>6</sup>, Jean Batiste Chouane<sup>6</sup>, Xin Liu<sup>1</sup>, Michael S. Roberts<sup>1,7</sup>✉, Xiaowen Liang<sup>1</sup>✉

1. Therapeutics Research Centre, The University of Queensland Diamantina Institute, The University of Queensland, Translational Research Institute, Woolloongabba, QLD 4102, Australia
2. Department of General Surgery, Changzheng Hospital, The Second Military Medical University, 415S, Fengyang Road, Shanghai, 200003, China.
3. Translational Research Institute, QLD 4102, Australia
4. School of Biomedical Sciences, The University of Queensland, St Lucia, QLD 4072, Australia
5. School of Environment and Biological Engineering, Nanjing University of Science and Technology, Nanjing, Jiangsu 210094, China
6. Department of Pharmacy, University of Rennes 1, Ille-et-Vilaine, Rennes, 35043, France
7. School of Pharmacy and Medical Science, University of South Australia, Adelaide, SA 5001, Australia

✉ Corresponding authors: E-mail: m.roberts@uq.edu.au and x.liang@uq.edu.au

© Ivyspring International Publisher. This is an open access article distributed under the terms of the Creative Commons Attribution (CC BY-NC) license (<https://creativecommons.org/licenses/by-nc/4.0/>). See <http://ivyspring.com/terms> for full terms and conditions.

Received: 2017.09.19; Accepted: 2017.11.24; Published: 2018.02.02

## Abstract

Indocyanine green (ICG) is a near-infrared dye that has been used in the clinic for retinal angiography, and defining cardiovascular and liver function for over 50 years. Recently, there has been an increasing interest in the incorporation of ICG into nanoparticles (NPs) for cancer theranostic applications. Various types of ICG-incorporated NPs have been developed and strategically functionalised to embrace multiple imaging and therapeutic techniques for cancer diagnosis and treatment. This review systematically summaries the biodistribution of various types of ICG-incorporated NPs for the first time, and discusses the principles, opportunities, limitations, and application of ICG-incorporated NPs for cancer theranostics. We believe that ICG-incorporated NPs would be a promising multifunctional theranostic platform in oncology and facilitate significant advancements in this research-active area.

## Introduction

Theranostics is a novel strategy with significant clinical potential that combines diagnostics and therapeutics to improve patient outcomes and safety through a more personalized approach [1, 2]. Biocompatible functional nanoparticles (NPs) provide a platform for simultaneous multimodal imaging-guided cancer therapy [3]. These NPs can incorporate chemo-, radio- or gene therapeutics and imaging probes, with appropriate intrinsic physicochemical properties, allowing early diagnosis and evaluation of treatment efficacy of cancer [2]. At present, various NPs such as magnetic NPs, quantum dots, and silica NPs are in development as theranostic agents for cancer. A number of NP therapeutics, imaging agents, and technologies have been approved for clinical use, with a large number in pre-clinical studies for both

imaging and therapy [4].

Indocyanine green (ICG) is an amphiphilic cyanine dye that was approved by the Food and Drug Administration (FDA) in 1954 for clinical applications [5], such as evaluation of cardiac output and hepatic function in patients. In the 1970s, protein-bound ICG was found to have strong absorption in the near-infrared (NIR) spectra, making it suitable for bio-imaging applications with high signal-to-background ratio due to low absorption of NIR spectra by biological tissues [6, 7]. In addition, ICG can be used as a photosensitizer to generate reactive oxygen species (ROS), such as singlet oxygen and superoxide to damage cancer cells by light illumination [8]. The absorbed light can also heat the cellular microenvironment, generating localised

hyperthermia and thereby destroying cancer cells [9]. Hence, ICG has been considered as a promising theranostic agent. However, ICG has some limitations including concentration-dependent aggregation, short half-life, poor photostability, poor hydrolytic stability, non-specific binding to proteins, and non-specific targeting [9], restricting its further theranostic application in cancer treatment. Incorporating ICG into NP platforms is a promising way to overcome these limitations. Although some theranostic nanomaterials have been proposed and developed, there are only scattered reports on the detailed applications and limitations of these nanomaterials in cancer theranostics. The scope of this comprehensive review is to first systematically summarise the properties and biodistribution of various types of ICG NPs, and discuss the principles, opportunities, limitations, and application of ICG NPs for cancer imaging and treatment.

### ***In vivo* biodistribution of ICG NPs**

ICG can be loaded, doped, or conjugated to the most relevant NP structure such as lipid-based NPs, polymer-based NPs, magnetic NPs, and mesoporous silica NPs [10-20]. These can all be further functionalised with a targeting moiety, therapeutic, and contrast agent. Figure 1 shows a schematic illustration of three typical types of ICG NPs. Since NPs have been extensively studied as ICG theranostic carriers, Table 1 summarises recent studies and the types and physicochemical properties of ICG-incorporated NPs, their ICG loading efficiency (LE) or encapsulation efficiency (EE), and *in vivo* biodistribution. The physicochemical properties of these ICG NPs in general are 10-200 nm in size, and are mostly injected intravenously in rodent models. The biodistribution of these ICG NPs are variable and dependent on physicochemical properties of the nanopatform such as size, charge, and surface coating.

### **Lipid-based ICG NPs**

Lipid-based NPs have been developed as drug carriers for cancer therapy. Although most NPs are used in pre-clinical models, some have entered human use, with the first class being liposomes as drug delivery carriers. Liposomes are closed spherical vesicles composed of a lipid bilayer made of either synthetic or natural phospholipids with diameters of about 100 nm [21]. Liposomes are widely used as delivery carriers due to their unique ability to encapsulate both therapeutic and diagnostic agents, which can protect the inside agents from *in vivo* environments, be functionalised with targeting ligands for tumor-specific delivery, and prolong

circulation time in the body [21]. Liposomal ICG can be engineered on molecular self-assembly principles and be made entirely of clinically-approved components [15]. The biodistribution of these clinically used PEGylated liposomes incorporating ICG was investigated by NIR fluorescence and multi-spectral optoacoustic tomography (MSOT) [15]. Compared to free ICG, liposome-ICG showed higher optical stability *in vivo*. At 24 h post-injection, strong fluorescence signals in the liver indicated that liposome-ICG mainly localised within that site. Clear optoacoustic signals were also seen in the liver by MSOT imaging, consistent with NIR imaging. Furthermore, MSOT revealed that liposome-ICG would transiently pass through the spleen, while no significant signals were detected in the kidneys [15]. Since drug EE is an important parameter for clinical application, the EE of ICG encapsulated into liposomes was measured in this study, which was 36%-46% according to the different concentrations of ICG [15].

Lipid NPs appear as nanocarriers for drug delivery, and are composed of bioassimilable ingredients with low toxicity. The particle size can be tailored according to the formulation composition, especially for lipid to surfactant ratio [13]. Given that ICG is an amphiphilic dye, it can be loaded both inside the lipid core and at the interface of lipid NPs. The pharmacologic and toxicological characteristics of ICG-loaded lipid NPs have been intensively investigated in Beagle dogs [12]. After systematic administration, plasma fluorescence continuously decreased, whereas fluorescence signals mainly occurred in the liver and to a lesser extent in the steroid-rich organs such as adrenal and ovaries, intestines, kidneys, and lymph nodes. No evidence of acute or delayed, hepatic, renal or hematological toxicity was observed at 1-, 5-, or 10-fold adapted doses [12]. In addition to systemic administration, ~50 nm ICG-loaded lipid NPs were found to be mostly accumulated in lymph nodes within 4 h after intradermal injection [11]. Furthermore, Mérian et al. demonstrated a different organ distribution profile for ICG-lipid NPs-<sup>14</sup>C after intravenous injection using fluorescence imaging and quantitative radioactivity [13]. ICG fluorescence was found to accumulate in liver, guts, and kidneys while radiotracer cholesteryl-1-<sup>14</sup>C-oleate ([<sup>14</sup>C]CHO) was retained in the liver, ovaries, and adrenals. Based on ICG fluorescence signals, ICG lipid NPs had the same distribution pattern as free ICG, indicating a total and immediate leakage of ICG after systemic injection, although the EE of ICG in NPs was 75%. *In vitro* experiments showed ICG leakage was strongly

affected by the presence of bovine serum albumin (BSA) and high affinity of ICG to plasma proteins [13]. Therefore, concerning the further application of ICG NPs, strategies based on ICG-loaded nanocarriers

have to overcome the high affinity of the dye for plasma proteins, leakage of ICG, and destabilization of nanosystems.

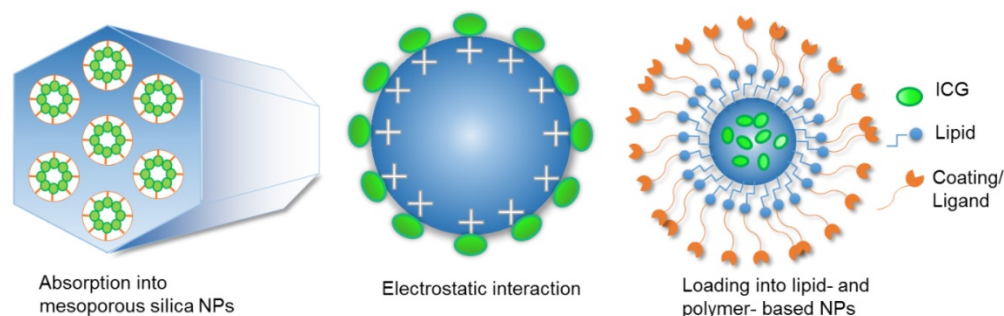


Figure 1. Schematic illustration of three types of ICG NPs.

Table 1. *In vivo* biodistribution of ICG NPs

NP Type	Size	Surface coating/ligand	ICG LE or EE (%)	Animal model	Administration routes	Observation time (h)	Fate of ICG-NPs	Detection methods	Ref
Lipid-based NPs	~50nm diameter	PEG-stearate co-surfactants	LE 77	Nude mice	Intradermally injected into paws	Up to 120	Lymph nodes, liver	Multichannel fluorescence imaging	[11]
	~50 nm	PEG	-	Beagle dogs	Intravenously injected through the cephalic vein.	24 and 72	Mainly distributed in the liver and less in the steroid-rich organs, intestines, lymph nodes, and kidneys	NIR imaging.	[12]
	50 nm diameter	Polymer coating	EE 74 ± 5	FVB female mice	Tail vein injection	Up to 24	Accumulated in liver, guts, and kidneys.	Fluorescence	[13]
	100-150nm	PEGylated	EE 36-45	CD-1 albino female mice	Tail vein injection	0.083, 1, 5, and 24 0.083, 4 and 24	Radiotracer was retained in liver, ovaries and adrenals. Strong signal in liver.	Radioactivity NIR imaging	[15]
Polymer-based NPs	90 ± 12	dextran (40 kDa)	EE 61 ± 3	Swiss webster mice	Intravenous injection	Up to 1	Accumulated in reticuloendothelial system; capsule's coating influences biodistribution	Fluorescence quantity	[10]
	465 ± 156	dextran (40 kDa)	EE 56 ± 3						
	97 ± 13	Fe3O4 NPs	EE 60 ± 2						
	39, 68, and 116 nm	PEG	EE 28-40 LE ~ 6.7	Female BALB/c nude mice	Tail vein injection	24	Distributed in liver, spleen, Lung, and kidneys; 68 nm NPs showed the most retention in tumor.	Fluorescence imaging	[14]
	~77 nm	PEG (5 kDa)	-	Female Swiss Webster mice	Tail vein injection	Up to 1	Prolong the circulation time of ICG; delayed its hepatic accumulation.	Fluorescence imaging.	[16]
Mesoporous silica NPs	50-100 nm	TA	-	Male Sprague Dawley rats	Intravenous injection	6	Mainly distributed to the liver and were taken up by the Kupffer cells.	Optical imaging, ICP-MS, and TEM	[17]
	50-100 nm	TA	-	Male nude mice or Sprague Dawley rats	Tail vein injection.	3	Positively charged NPs were quickly excreted from the liver into the GI tract, while negative ones remained within the liver.	NIR imaging	[18]
Iron oxide NPs	~25 nm	Milk protein casein	-	Nude mice	Oral administration	3, 5, 7	Distributed from stomach to ileum and further spread in intestines; NPs sustained in acidic gastric conditions.	NIR optical imaging/ MRI	[19]
Calcium phosphate NPs	~80 nm	PEI	LE 90	Swiss albino mice	Tail vein injection	0.083 to 48	Accumulated in the liver and retention was reduced with PEGylation.	NIR imaging, nuclear contrast imaging, and magnetic imaging	[20]

GI tract: gastrointestinal tract; MSOT: multi-spectral optoacoustic tomography; MRI: magnetic Resonance Imaging; PEG: polyethylene glycol; TA: trimethylammonium; NIR: near-infrared; PEI: polyethyleneimine; EE: encapsulation efficiency; LE: loading efficiency.

## Polymer-based ICG NPs

Polymeric NPs are a class of nanocarriers established for numerous drug delivery applications, and can be formulated by conjugating multiple functional units to soluble macromolecules or by co-polymer self-assembly [21]. Poly (lactic-co-glycolic acid) (PLGA) carriers approved by FDA are one of the most common biodegradable and biocompatible systems to load ICG for theranostic application. To explore size effects on the biodistribution and tumor accumulation of ICG polymeric NPs, Zhao et al. developed ICG loaded PLGA-lecithin-polyethylene glycol (PEG) core-shell NPs of 39 nm, 68 nm, or 116 nm in size via single-step nanoprecipitation [14]. After intravenous injection into pancreatic carcinoma xenograft mice, free ICG was quickly excreted and cleared from the living system, while all three types of NPs were retained within the living body for a long time, as detected by fluorescence imaging. ICG PLGA NPs of different sizes showed similar biodistribution patterns, where the liver, spleen, lung, and kidneys were the major organs [14]. These findings further revealed a size-dependent tumor accumulation of ICG PLGA NPs, where the 68 nm particles had efficient retention in tumors since they could easily pass through the vessel pores (~110 nm), and had slower clearance than the 39 nm ones. Another study investigated the influence of surface coating and size on the biodistribution of mesocapsules containing ICG *in vivo* [10]. Unlike polymeric NPs, which are composed of a solid colloidal polymer matrix with molecules or drugs are embed throughout the particles, the ICG within mesocapsules remain confined primarily to the polymer-salt aggregate core by electrostatic attraction. These mesocapsules can be coated with either a porous shell of NPs or a continuous film of polymer. In addition, neither the coating material of the capsules nor their size appeared to influence ICG EE in mesocapsules. In this study, ICG was administered intravenously to mice as a free solution or encapsulated within mesocapsules coated either with dextran of 100 nm or 500 nm diameter or ferromagnetic iron oxide NPs of 100 nm diameter. At 10 min following injection, free ICG was transported to the bile ducts while mesocapsule-ICG was retained in the liver up to 60 min post-injection. Mesocapsule-ICG was more likely to accumulate in the reticuloendothelial system as compared to free ICG. Interestingly, iron oxide NP-coated mesocapsule-ICG (100nm) had a greater distribution in the lung than either the 100 nm or 500 nm dextran mesocapsule-ICG [10]. Their results suggest that the uptake of particulate matter is more dependent on the surface coating than the size of the particles.

## Mesoporous silica ICG NPs

Mesoporous silica NPs (MSNs) with high surface area and pore volume have considerable biocompatibility and can easily be functionalised for a broad spectrum of biomedical applications [22]. Lee et al. were the first to synthesise MSNs functionalized with ICG to demonstrate their applicability for *in vivo* optical imaging [17]. The high dispersion of ICG molecules in the large surface areas of MSN could prevent them from aggregating and decrease fluorescence self-quenching. Additionally, the nanochannels of MSN have a confined space that can protect ICG from irreversible degradation and diminish the immune response [17]. In this study, they encapsulated ICG inside the nanochannels of MSN then probed the biodistribution of MSN in rats after intravenous administration. Strong and stable fluorescence of MSN-ICG was prominent in the liver as assessed by their in-house-built optical imaging system. More than 35% of silicon was revealed in the liver by ICP-MS analysis, which confirmed the findings from fluorescence imaging. MSN were further observed to be taken up by Kupffer cells in the reticuloendothelial system of the liver 3 h after injection by transmission electronic microscopy (TEM). In particular, MSN were found concentrated in the intracellular vesicles of Kupffer cells [17]. They performed a further study to determine if the surface charge of MSN-ICG played an important role in its biodistribution, clearance, and excretion [18]. MCM-41 mesoporous silica was selected to incorporate ICG due to its large surface area (~1000 m<sup>2</sup>/g), large pore volume (~1.0 cm<sup>3</sup>/g), and highly ordered hexagonal pore structure with adjustable pore size (1.5-30 nm) [18]. Positively charged MSN-ICG particles and negatively charged ones were synthesized and intravenously injected into nude mice. *In vivo* biodistribution imaging showed positively charged MSN-ICG were quickly excreted from the liver into the gastrointestinal tract (GI) tract, while negative ones remained in the liver. A similar distribution pattern was also found in Sprague Dawley rats, indicating that hepatobiliary transport of MSN-ICG NPs is particle- rather than animal-dependent. Taken together, excretion and clearance of MSN-ICG NPs can be regulated by the surface charge of particles, and positive ICG NPs are more easily be eliminated from the body compared to negative ones.

## Other ICG NPs

Iron oxide NPs with appropriate surface chemistry have been widely used for numerous *in vivo* applications such as magnetic resonance imaging (MRI), tissue repair, drug delivery, and detoxification of biological fluids [23]. Huang et al. developed a

novel drug delivery system composed of layer-by-layer (LBL) milk protein casein-coated iron oxide NPs [19]. ICG was selected as a model fluorescent molecule to be incorporated into the inner polymeric layer and subsequently coated with casein. The casein-coated iron oxide NPs were stable in the acidic gastric condition in the presence of gastric protease. LBL nanocarriers containing ICG were orally delivered to mice and *in vivo* imaging revealed this nanocarrier system could pass the stomach without significant degradation and accumulate in the small intestine. Therefore, ICG contained LBL milk protein casein-coated iron oxide NP is a promising nanoplatform for oral drug delivery, especially for drugs that are insoluble in water or degradable in the gastric environment. ICG offers NIR contrast capability for *in vivo* imaging guided drug delivery.

Calcium phosphate is the mineral component of human bones and teeth, and has been clinically applied for bone tissue regeneration [20]. Recently, calcium phosphate NPs have been developed for diagnostic, drug, gene or siRNA delivery systems with the advantage of having non-toxic components [20]. It has been reported that calcium phosphosilicate NPs have improved ICG loading efficiency and quantum yield compared to polymeric NPs [24]. In one study, calcium phosphate NPs were doped with both ICG and gadolinium ( $Gd^{3+}$ ), and labelled with 99m-technetium-methylene diphosphonate for combined optical, magnetic, and nuclear imaging [20]. The leaching-out of ICG was protected by a coating of polyethyleneimine (PEI). Similar to previous findings, free ICG were almost completely cleared from the body within a short time after intravenous injection, while ICG NPs were distributed in various organs such as the liver with relatively higher signals by NIR imaging. It is noted that retention of ICG-NPs in the liver was reduced with PEGylation and clearance was observed within 48 h without causing any major histopathological changes in key organs [20].

Overall, lipid- and polymer- based NPs are widely used as carriers to load ICG, with functionalised modifications for specific organ or tumor targeting. ICG LE or EE has been measured for lipid- and polymer- based NPs but not all types of NPs. Administration routes and physiochemical properties of NPs are key factors affecting ICG NP biodistribution, with surface coating playing a more important role than size. By manipulating synthetic parameters, the distribution of ICG NPs may potentially be controlled. It should be noted that strategies based on ICG-loaded NPs have to overcome the issue of ICG leakage in the living system by additional surface coating. Among ICG-loaded NP

carriers, biodegradable and biocompatible carriers such as PLGA and liposomes are the most common systems for potential clinical application.

## ICG NPs in cancer and lymph node imaging

Imaging modalities play an important role in cancer screening, diagnosis, treatment planning, and monitoring of treatment response. Near-infrared fluorescence (NIRF) imaging has numerous favourable characteristics including *in vivo* deep tissue penetration, high sensitivity, high resolution and multi-detection capability [25]. Another emerging noninvasive technique for *in vivo* deep tissue imaging is photoacoustic (PA) imaging. This type of imaging involves detection of acoustic waves generated from thermal expansion of endogenous contrast agents (e.g., haemoglobin, melanin) or exogenous contrast agents such as various dyes and NPs [26, 27] following absorption of low-energy nanosecond laser pulses. Since NIRF and PA signals can be generated from use of a NIR laser source (700-900 nm), they share some common exogenous contrast agents including NPs and fluorescent dyes such as ICG. There are some essential elements to NIRF in clinical imaging settings including excitation light produced by lasers for deep tissue penetration, safety of imaging agents for use in humans, selective targeting of disease markers, optical lenses and filters required to block the scattered excitation light emanating from the tissue, and sensitive charge coupled devices used for efficient collection of fluorescence [28]. Most human NIRF imaging studies employ ICG as imaging contrast within the blood and vasculature, which can be used to assess vascular repair intraoperatively [28]. For cancer imaging, ICG has been used for sentinel lymph node (SLN) mapping and identification of solid tumor margins during surgery [29-31]. SLNs are the initial draining lymph nodes of tumors. Therefore, SLN mapping is often used in an effort to detect cancer metastasis and is requisite for cancer staging, prognosis prediction and therapy selection. Success in SLN mapping with ICG has been demonstrated in gynaecological (e.g. cervical, vulvar, endometrial), skin, and gastric cancers [30, 32, 33]. Using ICG to identify solid tumor margins in humans has shown some preliminary success in liver metastasis, hepatocellular carcinoma, and lung and chest tumors [34, 35]. However, a limitation is the difficulty in distinguishing inflamed tissue from cancerous tissue. In addition, ICG extravasates passively into tumor tissues due to the "enhanced permeability and retention" (EPR) effect. This passive targeting mechanism might not be ideal for specific detection of tumor margins as the signals might be non-specific.

The use of ICG for tumor imaging is limited by several inherent properties of ICG, although some of them could be overcome by conjugation of ICG to NPs. For example, ICG has a low fluorescence quantum yield in aqueous solution due to self-quenching [36] and is quickly eliminated from the body through the liver after intravenous administration [37]. A potential approach to overcome these disadvantages of ICG imaging is to deliver ICG with NP systems to enhance ICG stability and circulation time and to facilitate ICG tumor accumulation. Table 2 summarises reported types of ICG NPs with their *in vivo* application for tumor and lymph node imaging.

### ICG NPs for NIRF imaging

For NIRF imaging, ICG is typically embedded into nanomaterials composed of polymer and inorganic matrices through non-covalent or covalent combination with a core-shell architecture. As mentioned above, these ICG NPs show enhanced photostability, biocompatibility and tumor accumulation, low self-aggregation, and usually brighter fluorescence signal compared to free ICG dye due to the protective architecture. Different preparation strategies have been employed in recent years to obtain functional ICG-NPs with different properties. A recent study by Song et al. reported the design and development of ICG loaded small-sized magnetic carbon NPs (MCNPs) for NIRF/MRI dual-modal imaging and photothermal therapy of breast cancer [38]. MCNPs were generated by growing iron oxide NPs *in situ* on carbon NPs by oxidation of activated carbon. ICG was then loaded onto MCNPs via physisorption, leading to increased photostability and enhanced photothermal effect. *In vivo* NIRF imaging monitored the accumulation of these ICG-loaded MCNPs in the tumor and organs of tumor-bearing mice in real-time, and demonstrated efficient accumulation and long retention of these NPs in the tumor due to the EPR effect and small NP size. Improved fluorescence properties were observed for

ICG-encapsulating calcium phosphate NPs as well [24]. Encapsulation did not affect the maximum fluorescence peak but significantly enhanced emission intensity relative to the free ICG at elevated concentrations. The PEGylated calcium phosphate NP encapsulation also demonstrated prolonged circulation times with passive tumor accumulation through the EPR effect in an *in vivo* breast cancer xenograft model [24]. This type of NPs is biocompatible and colloiddally stable in physiological solutions. With improved fluorescence, it might be suitable for sensitive, early stage diagnostic imaging of tumors. In another study, ICG was embedded in calcium phosphosilicate NPs composed of an amorphous calcium phosphate matrix doped with silicate [39]. These NPs were further bioconjugated with anti-transferrin receptor antibody to target transferrin receptors, which are highly expressed on breast cancer cells, or with short gastrin peptides to target gastrin receptors, which are overexpressed in pancreatic cancer lesions [39]. *In vivo* NIRF imaging demonstrated selective and effective targeting of these NPs in a model of breast cancer and pancreatic cancer with a potential for targeting across the blood brain barrier [39]. ICG has been loaded together with technetium-99m into polyamidoamine-based functionalized silica NPs for depicting deeply situated sentinel nodes [40] and imaging of HER2-expressing breast cancer [41] using NIRF imaging combined with radionuclide imaging. This dual-modality imaging system allowed deep tissue imaging and simultaneous visualization at anatomy resolution within the region of interest. Highly loaded ICG MSNs were used for accurate tumor border delineation and sensitive detection of tumor residuals during liver cancer surgery, which was attributed to the high ICG-loading resulting in high contrast between tumor and normal tissues under NIRF imaging [42].

**Table 2.** ICG NPs for cancer and lymph node imaging

Imaging technique	NP Type	Size	Surface coating/ligand	Tumor/lymph node	Species	Administration Routes	Ref
Near-infrared fluorescent imaging	Magnetic carbon	~10 nm	BSA	Breast tumor	Balb/c nude mice	Tail vein injection	[38]
	Calcium phosphate	16 nm	PEGamine	Breast tumor	Nude mice	Tail vein injection	[24]
	Calcium phosphosilicate	~20 nm	Pentagastrin-avidin	Pancreatic tumor	Athymic nude mice	Tail vein injection	[39]
	Silica	30-50 nm	<sup>99m</sup> Tc	Sentinel lymph node	Wistar rats	Tongue	[40]
	Silica	60-80 nm	PAMAM	Breast tumor	Athymic nude mice	Tail vein injection	[41]
	Mesoporous silica	<100 nm	Arginine-glycine-aspartic acid	Liver tumor	Balb/c nu/nu mice	Tail vein injection	[42]
	Micelles	20-30 nm	Pluronic F-127	Colon tumor	Balb/c mice	Tail vein injection	[43]
	DSPE-PEG	20-40 nm	FA	Breast tumor	Balb/c nude mice	Tail vein injection	[45]
	PLGA-lipid	~102.4 nm	FA	Breast tumor	Balb/c nude mice	Tail vein injection	[91]
	Lactosome	40-50 nm	PS-PLLA	Lymph node	Balb/c nude mice	Tail vein injection	[47]

Imaging technique	NP Type	Size	Surface coating/ligand	Tumor/lymph node	Species	Administration Routes	Ref
Photoacoustic imaging	HA-derived	80-260 nm	Aminopropyl-1-pyrenebutanamide; aminopropyl-5 $\beta$ -cholanamide; octadecylamine	metastases of gastric cancer Breast tumor	Athymic nude mice	Tail vein injection	[46]
	Nanogel	188 nm	HA	Breast tumor Sentinel lymph nodes	Nude mice	Intravenous injection Intradermal injection	[44]
	Liposome	191 nm	DSPE	Brain tumor	Fisher 344 rats	Tail vein injection	[48]
	SWNT	1-2 nm diameter and 50-300 nm length	Cyclic RGD peptides	Brain tumor	Nude mice	Tail vein injection	[55]
	SPIO	28 nm	DSPE-PEG2000	Breast tumor	Balb/c mice	Intravenous injection	[56]
	PLGA-lipid	118.7nm	FA	Breast tumor	Balb/c nude mice	Tail vein injection	[25]
	Liposomes	120-130 nm	PEG	Colon tumor	CD-1 albino mice	Tail vein injection	[15]

BSA: bovine serum albumin; SWNT: single walled carbon nanotubes; FA: folic acid; PLGA: poly (lactic-co-glycolic acid); DSPE-PEG2000: 1,2-distearoyl-sn-glycero-3-phosphoethanolamine-N-[methoxy (polyethylene glycol)-2000]; SPIO: superparamagnetic iron oxide; PS-PLLA: poly(sarcosine)-poly(L-lactic acid); DSPE: 1,2-distearoyl-sn-glycero-3-phosphoethanolamine.

In addition to inorganic matrices, ICG has also been encapsulated into polymer-based [43-47] and liposome-based nanomaterials [48]. Encapsulation of ICG within polymeric micelles formed from the thermosensitive block copolymer Pluronic F-127 showed similar effects as ICG-loaded calcium phosphate NPs, such as prolonged *in vivo* circulation time and enhanced fluorescence stability of ICG. NIRF whole-body imaging demonstrated the passive targeting of this type of micelle to solid tumors via the EPR effect in colon carcinoma tumor-bearing mice. As both Pluronic F-127 and ICG are already FDA approved, this type of micelle may easily be applied in clinical situations. To overcome the limitation of free ICG, Zheng et al. [45] prepared biodegradable folic acid-targeted NPs encapsulating ICG (FA-INPs) with intrinsic FA-targeting ligands. The FA-INP showed enhanced ICG stability, produced stronger temperature response than free ICG and exhibited significant targeting to breast tumors in *in vivo* studies as shown in Figure 2. This makes the system promising as a theranostic agent for imaging guided cancer photothermal therapy clinically. For imaging-guided tumor surgery, liposomes formulated with phospholipid-conjugated ICG, and ICG-loaded hyaluronic acid (HA)-derived NPs were designed for application in models of brain [48] and breast [46] cancer, respectively. Both NP formulations showed tumor-specific biodistribution and stronger contrast enhancement for tumor tissues compared to free ICG. Different strategies for development of ICG NPs were applied to achieve selective imaging of metastatic lymph nodes using NIRF imaging. Tsujimoto et al. [47] established theranostic photosensitive "lactosome", which is a micelle assembled from block copolymers, poly(sarcosine)-poly(L-lactic acid) (PS-PLLA), loaded with ICG. They demonstrated selective lactosome

accumulation in metastatic lymph nodes in a gastric cancer model due to the EPR effect using NIRF imaging and showed photodynamic therapeutic effect. In contrast, free ICG could not reveal metastatic lymph nodes in the same model using NIRF imaging. In another study, Mok et al. [44] designed ICG-incorporated HA nanogels for selective imaging of tumors and metastatic lymph nodes by hyaluronidase (HAdase)-based activation. ICG fluorescence was quenched in HA-ICG nanogels, but could be turned on in the presence of exterior HAdase. Therefore, this type of HA-ICG nanogel is a promising probe for selective NIRF imaging of specific cancers and metastatic lymph nodes that overexpress HAdase. Enhanced photostability and accumulation of HA-ICG nanogels facilitated the long-term visualization of target tissues *in vivo* for diagnosis of cancer and metastatic lymph nodes.

In summary, there are different methods for ICG NP preparation to achieve enhanced tumor accumulation, prolonged circulation and improved stability to facilitate *in vivo* NIRF imaging. Nanomaterials selected to prepare ICG NPs are usually biocompatible with minimal toxicity and high potential for clinical translation. NIRF imaging is mainly used for imaging-guided surgery to identify tumor margins or metastatic lymph nodes. These NPs can also be used as theranostic NPs for imaging-guided cancer (photothermal or photodynamic) therapy in clinical applications. Breast cancer models seem to be the most commonly used cancer models for proof-of-concept in all reported studies.

### ICG NPs for PA imaging

The use of exogenous contrast agents to generate photoacoustic signals in tumor imaging has received much attention in recent years. Metals (most notably

gold) or semiconducting NPs, organic NPs (e.g. carbon), and small-molecule dyes are three main classes of PA contrast agents [49-52]. ICG is a small molecule dye that was rapidly adopted for cancer research studies using PA imaging for identification of sentinel lymph nodes in the lymphatic drainage from tumors [53]. However, free ICG could have substantial concentration- and environment-dependent changes in optical properties due to its hydrophobicity [54] as well as low sensitivity and photoinstability. Therefore, ICG NPs are prepared with the main focus of improving the photoacoustic signal of ICG. As for NIRF imaging, different strategies are applied to the design of NPs to achieve this purpose. However, compared to NIRF imaging, there are fewer reports of PA imaging for ICG NP application as this is a relatively new imaging modality with limited instrument options available.

In a study by de la Zerda et al. [55], ICG was attached to the surface of cyclic Arg-Gly-Asp (RGD) peptides conjugated to pegylated single-walled carbon nanotubes (SWNT-RGD) to achieve higher photoacoustic contrast in living tissues and to molecularly target  $\alpha_v\beta_3$  integrins, which are overexpressed in tumor vasculature (Figure 3A).

Compared to untargeted contrast agent and SWNTs, tumor targeting and higher photoacoustic signal of ICG SWNT-RGD were demonstrated in a tumor xenograft model after intravenous injection by PA imaging (Figure 3B). To enhance PA imaging contrast and address the rapid clearance and non-specific tissue binding issue of free ICG, Gao et al. [56] encapsulated ICG into degradable superparamagnetic iron oxide (SPIO) NPs coated with a lipid layer of 1,2-distearoyl-sn-glycero-3-phosphoethanolamine-N-[methoxy(polyethylene glycol)-2000] (DSPE-PEG2000). The long circulation time and the high tumor targeting efficiency of these NPs were demonstrated in breast tumor xenograft model by *in vivo* PA imaging. This type of NP could be potentially used in clinical applications for determining tumor margins as both SPIO and ICG are FDA approved agents. In another study by Wang et al. [25], ICG was encapsulated in biodegradable poly(D,L-lactide-co-glycolide) (PLGA) NPs with FA-targeting ligands. Their great tumor targeting capability for MCF-7 breast tumor and prolonged circulation time was demonstrated *in vivo* as well as their improved photoacoustic contrast. Incorporation of ICG into liposomal bilayers has also been reported to be an efficient way to improve tumor accumulation and photoacoustic signal [15].

In summary, ICG has been widely used for cancer and metastatic lymph node imaging using NIRF and PA imaging modalities in preclinical studies. Due to the limitations of free ICG, more and more ICG NPs are prepared to enhance its fluorescence or PA signal, photostability, *in vivo* circulation time and tumor targeting efficiency. These NPs can generally be divided into two classes: 1) metallic or inorganic NPs, and 2) polymer-based NPs; most of NPs are biocompatible and biodegradable with minimal toxicity. Several proof-of-concept preclinical experiments have demonstrated their suitability for cancer diagnosis and surgery. However, further clinical trials are necessary before their application in the clinic, and quality control criteria should be established for large scale production.

### ICG NPs for imaging-guided therapy of cancer

The development of multifunctional NPs that provide both diagnostic and therapeutic abilities has attracted recent

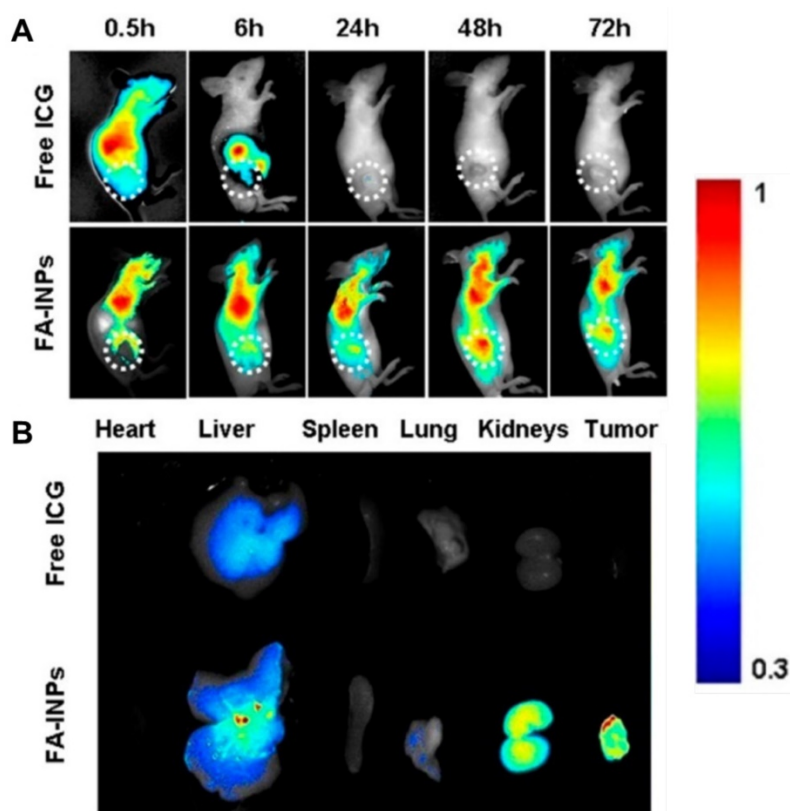


**Figure 2.** *In vivo* NIRF imaging of FA-INPs and free ICG in nude mice bearing MCF-7 tumors after intravenous injection. (A) Time-lapse NIRF images of nude mice (the tumors are circled with a dotted line) (B) NIRF images of organs and tumors 48 h post-injection of free ICG and FA-INPs. Reproduced with permission from ref.[45], Copyright 2017, ACS Appl Mater Inter.

attention. An ideal multifunctional ICG NP to be used for imaging-guided therapy in cancer would have abilities including: early visualization of tumors, effective delivery of drugs and theranostic agents, and optimised therapeutic strategy to reduce side effects [57]. Current development of ICG nanotheranostics leverages imaging modalities and incorporates them into various NP platforms along with different cancer therapeutics. We review recent ICG nanotheranostics that combine imaging with photothermal therapy, photodynamic therapy, or dual therapy of photothermal, photodynamic, and chemotherapy, which are summarised in Table 3. There are some possible mechanisms for delivery of ICG NPs into tumor tissues such as macrophage delivery and vesicle targeting. The standing mechanism of NP delivery is through leaky blood vessels of tumors via passive or active targeting strategies [58]. Passively targeted NPs have been shown to nonspecifically enter the tumor based on their size and shape [58]. Actively targeted NPs rely on passive targeting to reach the tumor, but could be designed to preferentially bind and/or be internalized by specific cancer cells. Since NPs with sizes larger than 100 nm are likely to be trapped in the extracellular matrix [59],

the size of ICG NPs are generally between 10-100 nm for efficient targeted therapy in cancer.

## ICG NPs for single modality therapy in cancer

### Photothermal therapy

Photothermal therapy employs photoabsorbers to generate heat from light absorption, resulting in thermal ablation of tumor cells [60]. Nowadays, photothermal therapy has emerged as an alternative treatment for cancer with minimal invasiveness compared to other cancer interventions [61]. ICG is recognised as an effective photosensitizer by NIR laser-excitation for photothermal therapy [45]. However, application of free ICG for photothermal therapy in cancer is limited by its concentration-dependent aggregation, short half-life, and poor stability *in vivo* [45, 62]. One idea is to use ICG loaded NPs to serve as energy transducers, which concentrate within tumor areas, and upon laser irradiation, can convert light into heat and kill adjacent cancer cells. Compared to conventional drug delivery, such a treatment paradigm occurs only within the illumination area, thus minimising normal tissue damage [63-65].

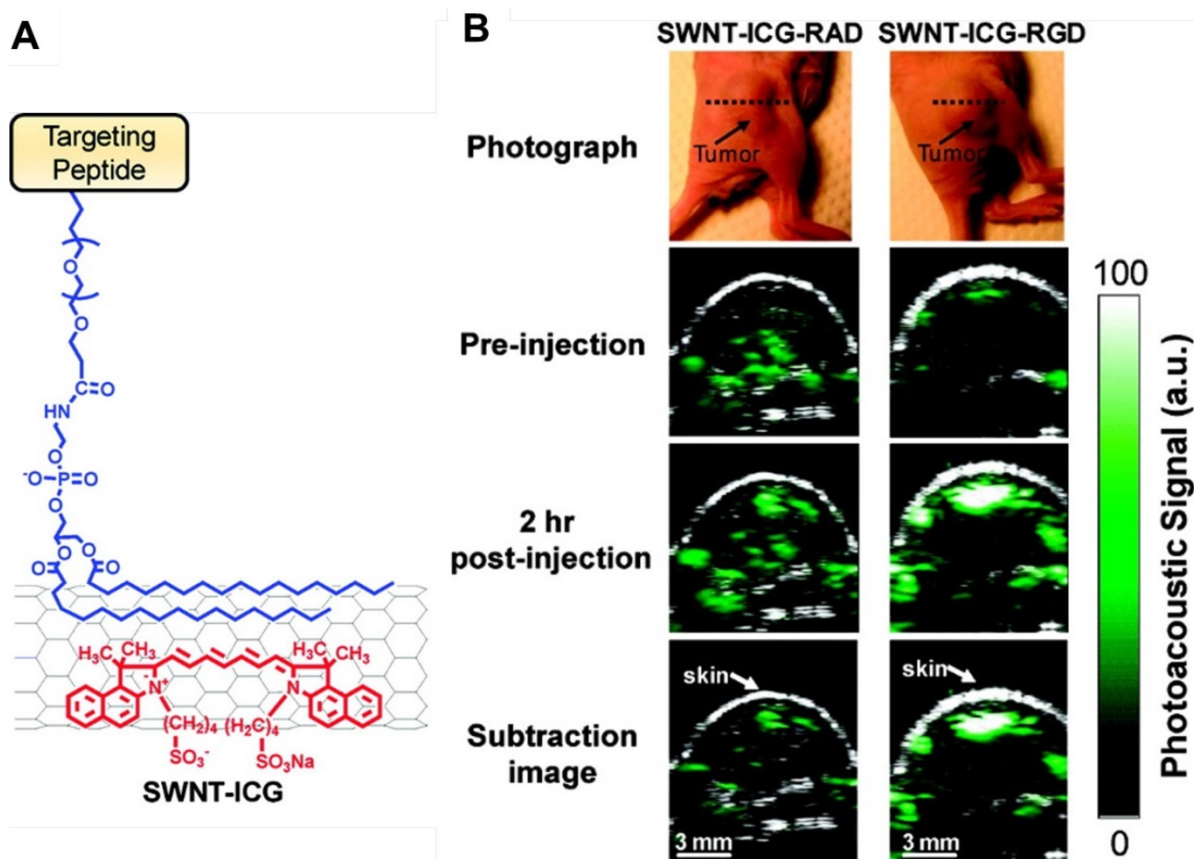


**Figure 3.** SWNT-ICG-RGD tumor targeting in living mice by PA imaging. (A) Illustration of SWNT-ICG NPs. ICG molecules (red color) attached to the SWNT surface via noncovalent  $\pi$ - $\pi$  stacking bonds. SWNT-ICG-RGD tumor targeting in living mice. (B) Ultrasound (grey) and photoacoustic (green) images of one vertical slice through the tumor as indicated by the dotted black line in the photograph. SWNT-ICG-RGD showed higher accumulation in the tumor compared to control SWNT-ICG-RAD. Reproduced with permission from ref. [55], Copyright 2017, *Nano Lett.*

**Table 3.** ICG NPs for imaging-guided therapy in cancer

Therapy type	NP Type	Size	Surface coating/ligand	Tumor type	Species	Administration Routes	Reference
Photothermal therapy	Biomimetic	200.4 nm	Cancer cell membrane	Breast tumor	Nude mice	Tail vein injection	[63]
	Magnetic carbon	10 nm	BSA	Breast tumor	Nude mice	Tail vein injection	[38]
	Mental-organic	100 nm	HA	Breast tumor	Female BALB/c mice	Tail vein injection	[65]
	SPIO	27.4 nm diameter	DSPE-PEG	Cervical carcinoma	Nude mice	Tail vein injection	[68]
	Magnetite nanocluster	50-200 nm	Poly(dopamine)	Liver tumor	Male nude mice	Tail vein injection	[61]
	Lipid	20-40 nm	FA	Breast tumor	Balb/c nude mice	Tail vein injection	[45]
Photodynamic therapy	PLGA	39, 68, 116 nm	PEG	Pancreatic carcinoma	Female BALB/c nude mice	Tail vein injection	[14]
	Lactosome	40-50 nm	-	Gastric tumor	Nude BALB/c mice	Tail vein injection	[73]
	Calcium phosphosilicate	~16 nm	CD117	Leukemia	C3H/HeJ mice	Intravenous injection	[77]
Photoacoustic therapy	Biomimetic artificial red cells	70 nm	DSPE-PEG	Breast tumor	Female BALB/c nude mice	Intratumoral injection	[74]
	PL-PEG	18 nm	FA	Breast tumor	Female BALB/c mice	Tail vein injection	[79]
Dual therapy (photothermal and photodynamic)	Mesoporous silica	~12 nm diameter	CuS	Breast tumor	Female nude Mice	Tail vein injection	[81]
	Liposomes	~115 nm	iRGD	Breast tumor	Female BALB/c mice	Tail vein injection	[82]
Dual therapy (chemo-phototherapy)	Liposomes	~43 nm	DSPE-PEG	Breast tumor	Female BALB/c nude mice	Intratumoral injection	[89]
	PLGA	86.3 nm	PEG	Breast tumor	Female BALB/c nude mice	Intratumoral injection	[87]
	PLGA	~221 nm	DSPE-PEG	Brian tumor	BALB/c nude mice	Intravenous injection	[86]

PL-PEG: phospholipid-polyethylene glycol; BSA: bovine serum albumin; SPIO: superparamagnetic iron oxide; DSPE-PEG: 1,2-distearoyl-sn-glycero-3-phosphoethanolamine-N-[methoxy (polyethylene glycol)]; iRGD: a cyclic nanopeptide with amino acid sequence of CRGDKGPDC; PLGA: poly(lactic-co-glycolic

On the basis of the ICG-loaded lipid and -polymer NPs discussed above, biomimetic NPs that were loaded with ICG and coated with cancer cell membrane showed specific homologous targeting to cancer cells with photothermal response and good fluorescence and photoacoustic imaging properties [63]. By NIR and PA dual modal imaging, *in vivo* dynamic distribution of these biomimetic ICG-loaded NPs was monitored with deep penetration and high spatial resolution. Under NIR laser irradiation, ICG-NPs exhibited highly efficient photothermal therapy to eradicate breast cancer xenograft tumors in mice, while there was no efficacy in inhibiting the growth of tumors by free ICG due to its rapid clearance and low accumulation in the tumor [63]. Another multifunctional cancer-targeted theranostic nanoplatform was developed by the growth of iron oxide magnetic NPs on carbon NPs loaded with ICG [38]. *In vivo* NIRF imaging revealed these ICG-loaded magnetic NPs could be targeted to the breast tumor site after intravenous injection. Subsequent photothermal therapy of tumor-bearing mice was achieved, as evidenced by significant ablation of the tumor [38].

HA, which is a natural, highly biodegradable, and biocompatible biopolymer, can mediate the targeting recognition of CD44 overexpressing in cancer cells [66]. HA-conjugated and ICG-loaded

metal organic NPs exhibited good NIR absorbance, low toxicity, high uptake in CD44 positive MCF-7 cancer cells, as well as efficient tumor targeting in breast cancer xenograft tumors [65]. *In vivo* photothermal therapy further demonstrated these newly developed ICG-loaded metal organic NPs can effectively inhibit the growth of MCF-7 tumors in mice after conjugation with HA. In addition to HA, FA is also a natural material with lower molecular weight and relatively high stability [60]. It has also been recognised as a potential targeting agent due to high expression of the folate receptor in some types of solid tumors such as breast, lung, and ovarian cancers [60, 67]. Some particles have been conferred with tumor-targeting specificity by incorporating FA to the particle surface [45]. A good example was shown by Zheng et al., where biodegradable FA-targeted ultra-small NPs encapsulating ICG with intrinsic FA-targeted ligands enabled efficient targeting and suppressed breast cancer xenograft tumors by photothermal therapy [45].

The application of MRI-guided tumor photothermal ablation is impeded by insufficient photothermal ablation and low accumulation of most nanomaterials in tumor tissues [61]. Wu et al. developed a magnetite nanocluster@poly(dopamine)-PEG@ICG nanobead for tumor MR imaging and photothermal therapy using a magnetite nanocluster

core coated with poly(dopamine), that was then conjugated with PEG and ICG was absorbed on the surface [61]. The tumor-homing ability of these developed nanomaterials was significantly enhanced, as shown by MRI, and photothermal ablation of liver tumors was more efficient at a relatively low dose. Another biodegradable theranostic NP was constructed for fluorescence and MR dual modal imaging-guided photothermal therapy by ICG-loaded SPIO NPs with a coating of DSPE-PEG [68]. In the study, *in vivo* MR and fluorescence imaging indicated high tumor targeting efficiency by these ICG-loaded SPIO NPs and effective tumor ablation by photothermal therapy in cervical carcinoma [68].

Conventional drugs have limited penetration into tumors, especially in poorly permeable tumors such as pancreatic and colon carcinoma [14]. The NP size could have a critical effect on passive tumor targeting and accumulation, which would influence their therapeutic efficacy. It has been shown that smaller NPs rapidly diffuse through tumor matrix and have better penetration [69]. As discussed previously, to explore the effects of NP size on tumor accumulation and therapeutic efficacy, Zhao et al. developed PLGA ICG NPs 39 nm, 68 nm, and 116 nm in size for *in vivo* photothermal therapy in a xenograft pancreatic carcinoma model [14]. *In vivo* imaging revealed the 68 nm ICG NPs possessed the best passive targeting efficiency and highest ICG accumulation in tumor tissue, while the 116 nm particles could not penetrate vessel pores in sinusoids and the 39 nm ones were easily eliminated from tumor tissues. Photothermal therapy further illustrated 68 nm ICG NPs had the strongest efficiency in suppressing tumor growth due to their highest accumulation in the tumor [14].

In summary, diagnostic imaging and photothermal therapy can be integrated into a single procedure. ICG-loaded NPs can serve as an excellent nanoplatform and size-dependent theranostic model for passive tumor targeting and imaging-guided photothermal therapy in cancer. To combine PA, MR, and NIR multimodal imaging capabilities with ICG as an anticancer photosensitive agent under NIR laser irradiation, ICG can be loaded into diverse types of nanomaterials for simultaneous imaging and photothermal therapy.

### Photodynamic therapy

Photodynamic therapy has been known as an alternative cancer treatment to chemotherapy or radiation therapy, and consists of three components: a photosensitizer, light, and oxygen. Once a photosensitizer is activated by laser light of a specific wavelength, it can react with endogenous oxygen to

generate intracellular singlet oxygen to kill tumor cells [70]. Photosensitizers can selectively target tumor cells to reduce side effects on normal cells, and photodynamic therapy does not induce any chemoresistance, showing advantages over radiation and chemotherapy. Photodynamic therapy has been clinically applied in poor surgical candidates with advanced cancers [71]. Many photosensitizers have been developed; however, only a few have been applied to clinical trials due to non-specific tumor targeting, low extinction coefficients, and absorption spectra at relatively short wavelengths. As described above, ICG is an ideal photosensitizer as it has a strong absorption band between 700 and 800 nm, which enables deep light tissue penetration without significant heating [72]. In one study, ICG loaded into lactosomes 40-50 nm in size was used as a photosensitizer in photodynamic therapy for peritoneal dissemination of gastric tumor in nude mice [73]. ICG-lactosomes selectively targeted the tumor site after intravenous injection. Photodynamic therapy significantly reduced the weight of the disseminated nodules, limited weight loss, and improved survival rates of mice with gastric tumors. To overcome the challenge of treating the hypoxic regions of tumors, Luo et al. developed biomimetic artificial red cells by loading haemoglobin to carry oxygen and ICG as photosensitizer for a boosted photodynamic strategy [74]. Upon exposure to NIR laser, ICG generated massive amounts of ROS with sufficient oxygen supply. In particular, haemoglobin was simultaneously oxidized into the active and resident ferryl-hemoglobin, which caused persistent cytotoxicity. Generated ROS and ferryl-hemoglobin synergistically triggered the oxidative damage of xenograft breast tumor leading to complete suppression.

In addition, *in vivo* photodynamic therapy is not limited to subcutaneous solid tumors residing in superficial locations since light can be delivered to internal organs using fibre optics [75]. One study successfully applied photodynamic therapy to an orthotopic glioblastoma rat model by delivery of polymeric NPs encapsulating photosensitizers specifically to the tumor site, with the laser source delivered through a hole created in the skull during surgery [76]. With regard to non-solid cancers of the blood and bone marrow, leukemia presents a challenge to delivering photosensitizer due to tumor manifestation throughout the body. Barth et al. developed calcium phosphosilicate ICG NPs as a photosensitizer and further conjugated them to specifically target CD117, a receptor tyrosine kinase for stem cell factor that is normally internalized by ligand binding [77]. CD117-targeted ICG NPs

significantly enhanced the efficacy of photodynamic therapy in a murine leukemia model following light irradiation of the spleen, resulting in 29% disease free survival [77]. Altogether, leukemia-targeted ICG-loaded NPs offer promise to effectively treat non-solid cancers.

### Photoacoustic therapy

Photoacoustic techniques can not only be used for high-efficiency photoacoustic imaging, but can also be applied for cancer therapy. As described above, photothermal therapy is applied to cancer using long continuous laser irradiation, whereas photoacoustic therapy for cancer destruction uses a pulsed laser [78]. Photoacoustic therapy for cancer treatment has some advantages, including reduced laser power for anti-cancer effect, improved therapy efficacy, and provides a mechanical mechanism for cell damage with less toxicity and drug resistance [79]. Zhong et al. has successfully employed ICG NPs functionalised with FA as cancer-targeting nanoprobes for breast cancer treatment using a photoacoustic technique [79]. During photoacoustic therapy, an optical parametric oscillator (OPO) operated at 808 nm with a pulse duration of 10 ns and a pulse repetition rate of 10 Hz was applied to treat the subcutaneous tumors [79]. The mouse tumors showed a much slower growth rate after photoacoustic treatment. Full body thermographic images were captured during photoacoustic therapy by an infrared camera. Only a small temperature increase was found in the tumor, which is entirely different from photothermal therapy that heat the ICG NPs in the tumor tissue to high temperatures for killing cancer cells. [79].

### ICG NPs for dual-modality therapy in cancer

#### Combined photothermal and photodynamic therapy

Dual-modality and multifunctional ICG NPs are being developed by attaching molecular moieties with imaging, therapeutic and targeting functions for simultaneous imaging and therapy of tumors. It has been reported that photodynamic therapy, which suppresses cancer cells by cytotoxic ROS or other radical species produced by the photosensitisers, can be combined with photothermal therapy for significantly improved therapeutic efficacy and decreased side effects [8]. As described above, ICG shows strong NIR absorbance and simultaneously achieves photodynamic and photothermal therapy effects under 808 nm laser irradiation [80]. Considering the properties of ICG as a photosensitiser, You et al. successfully loaded ICG into MSNs coated with copper sulfide (CuS), which simultaneously triggered photodynamic and

photothermal therapy effects with a single 808 nm laser [81]. The group treated with ICG NPs and light showed a 100% survival after 35 days in a 4T1 breast cancer mouse model, while the other treated groups had lower survivals. Overall, the single wavelength-triggered dual modality therapy of ICG NPs combining photothermal and photodynamic therapy achieved enhanced anticancer efficacy with a simplified treatment process and showed a promising tumor theranostic platform.

To achieve effective treatment by dual-modality therapy, Yan et al. developed internalised RGD (iRGD)-modified ICG liposomes for molecular imaging-guided simultaneous photodynamic and photothermal therapy against breast tumor [82]. iRGD modified ICG liposomes exhibited high stability, and enabled accurate and sensitive detection of breast tumors due to the high affinity of iRGD peptides for  $\alpha v \beta 3$  integrin, and their effective tumor-internalisation property [83]. These ICG liposomes showed higher tumor accumulation with tumor inhibition through simultaneous photodynamic and photothermal effects, with no tumor recurrence or obvious treatment induced toxicity.

#### Combined chemo- and phototherapy

Cancer treatments usually involve combined therapies of surgery, chemotherapy, radiotherapy, and phototherapy, which are dependent on the tumor location and stage of malignancy [84]. The combination of therapeutic approaches is considered a highly rational strategy for effective treatment of cancer. Chemotherapy is one of the most common therapies, with various chemotherapeutics loaded into nanocarriers for improving tumor targeting, reducing side effects and avoiding multi-drug resistance [85]. Hao et al. developed a multifunctional nanosystem for imaging-guided chemotherapy and phototherapy in which ICG and docetaxel were simultaneously loaded into PLGA NPs, as shown in Figure 4 [86]. These particles were further decorated by brain-targeted peptide angiopep-2 to achieve combined chemo-phototherapy for glioma under NIR guidance. The results showed imaging-guided chemo-phototherapy of ICG PLGA NPs efficiently prolonged the life span of brain orthotopic U87MG glioma mice due to the synergistic effects from docetaxel and photothermal therapy under 808 nm irradiation [86]. A similar study also employed PLGA NPs as a nanocarrier system for co-delivery of doxorubicin and ICG for breast cancer treatment by a combination of chemotherapy and photothermal therapy [87]. These NPs showed higher temperature response, faster doxorubicin release under laser irradiation, and longer accumulation time in mice

bearing breast tumors for synergistic anticancer therapy. Compared to chemo- or photothermal treatments alone, the combined treatment of chemo-photothermal therapy with laser irradiation synergistically induced apoptosis of doxorubicin-sensitive and -resistant cells, and suppressed tumor growth *in vivo*. Importantly, no tumor recurrence was found after only a single dose of ICG PLGA NPs with laser irradiation [87].

Photochemical internalisation refers to light-induced delivery of genes, proteins and therapeutic molecules [88]. ICG, as an amphiphilic photosensitizer could insert into the plasma membrane, then be taken up by endocytosis, where it would localize specifically in the membranes of endocytic vesicles [88]. Zhao et al. developed temperature-sensitive liposomes (TSL) co-encapsulating doxorubicin and ICG for synergistic chemo- and photothermal therapy of breast tumors [89]. After injection, TSL-ICG NPs were taken up by breast adenocarcinoma cells via endocytosis and TSL-ICG NPs caused hyperthermia through NIR laser irradiation to induce endosomal disruption, while doxorubicin was simultaneously released and entered the cell cytosol for increased cytotoxicity. TSL-ICG NPs exhibited laser-controlled release of doxorubicin in the tumor and completely eradicated tumors

without side-effects. Hence, the combination chemo-photothermal therapy is a promising strategy for cancer treatment.

### Current approaches and future perspectives

Theranostics is a novel concept that refers to the combination of diagnosis and therapy, and the use of nanomaterials for this purpose is emerging as a promising therapeutic paradigm in cancer. ICG, as a FDA-approved theranostic agent, has been effective in cancer treatment after being incorporated into nanoplateforms. ICG NP is a novel “Trojan horse” strategy to deliver simultaneous effects in cancer theranostics that overcome the challenge of accessing and treating the hypoxic regions of tumors and limitations of free ICG such as poor photostability, non-specific targeting, and short half-life. As we described above, the *in vivo* biodistribution and tumor targeting behaviour of ICG-based theranostic NPs can be monitored by NIR or PA imaging. ICG NPs can also be employed for various imaging-guided cancer therapies including photothermal, photodynamic, photoacoustic, and dual-modality therapy. Imaging can provide the biodistribution or the tumor targeting of the drug and photosensitizer to improve the optimal therapeutic timing and irradiation dosimetry. In addition to ICG, IR-780 iodide is a NIR fluorescent

heptamethine dye that exhibits preferential accumulation characteristics in the mitochondria of tumor cells [90], and could be considered as a promising tumor-targeting agent for cancer theranostics.

In this review, we have highlighted diverse theranostic nano-systems with integrated functions for cancer imaging and therapy. However, the choice of an appropriate nanoplateform is not clear since several factors can simultaneously affect biodistribution and tumor targeting. Successful targeting strategies of ICG NPs have to be determined experimentally on a case-by-case basis, which also requires suitable screening methodologies for determining optimal physiochemical characteristics of ICG NPs. Although considerable efforts have been directed to the development of theranostic

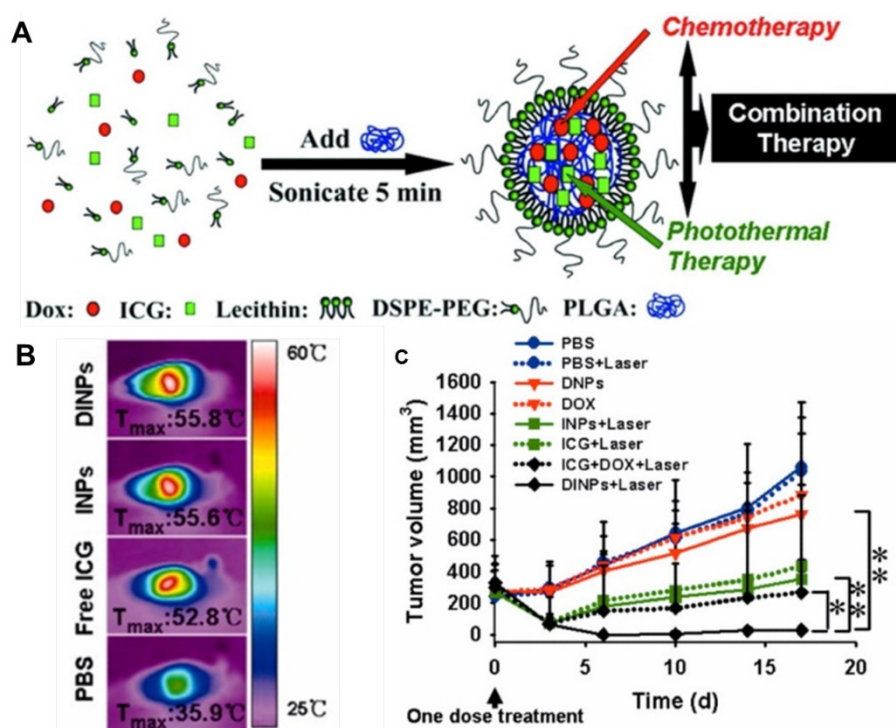


**Figure 4.** (A) Schematic illustration of the synthesis of doxorubicin- and ICG- loaded PLGA-lecithin-PEG NPs. (B) Infrared thermographic maps of mice intratumorally injected with DINP, INP, PBS, or free ICG measured at 5 min after irradiation. (C) MCF-7 tumor growth curves of different groups after dual-modality treatment. Reproduced with permission from ref. [87]. Copyright 2017, ACS Nano.

ICG-incorporated nanoplatforms and approaches, these ICG NPs have yet to be employed in a clinical setting. For clinical applications, in addition to enhancing the ability to image and target the location of tumors, it is imperative to provide appropriate therapeutic regimens and address the issues of safety and efficacy. In addition, limited depth penetration of the light that is used to excite laser-based imaging and therapy of ICG NPs may also obstruct their clinical applications for orthotopic tumors. It is noted that only one study reported the theranostic application of ICG NPs in non-solid cancer. In the case of circulating cancer cells such as leukaemia, a therapy that targets surface antigens with high affinity would be efficacious.

Several proof-of-concept preclinical experiments have demonstrated ICG NPs' applicability for cancer imaging and therapy. Continued research in theranostic ICG NPs has potential to solve the challenges discussed in this review. Specific surface coating and charge of ICG NPs will allow for tailored circulation time unique to the application. Use of naturally occurring systems allow for penetration of cell membranes much more efficiently than synthetic NPs. Biodegradable ICG NPs are an important alternative type to overcome toxicity and accumulation concerns.

## Abbreviations

ICG: indocyanine green; NP: nanoparticle; NIR: near-infrared; ROS: reactive oxygen species; LE: loading efficiency; EE: encapsulation efficiency; MSOT: multi-spectral optoacoustic tomography; [<sup>14</sup>C]CHO: cholesteryl-1-<sup>14</sup>C-oleate; BSA: bovine serum albumin; PLGA: poly (lactic-co-glycolic acid); PEG: polyethylene glycol; MSNs: mesoporous silica NPs; TEM: transmission electronic microscopy; GI: gastrointestinal tract; MRI: magnetic resonance imaging; LBL: layer-by-layer; Gd<sup>3+</sup>: gadolinium; PEI: polyethyleneimine; NIRF: near-infrared fluorescence; PA: photoacoustic; SLN: sentinel lymph node; EPR: enhanced permeability and retention; MCNPs: magnetic carbon NPs; HA: hyaluronic acid; PS-PLLA: poly(sarcosine)-poly(L-lactic acid); RGD: Arg-Gly-Asp; SWNT-RGD: single-walled carbon nanotubes; SPIO: superparamagnetic iron oxide; DSPE-PEG2000: 1,2-distearoyl-sn-glycero-3-phosphoethanolamine-N-[methoxy(polyethylene glycol)-2000]; CuS: copper sulphide; TSL: temperature-sensitive liposomes.

## Acknowledgements

The study was supported by grants from National Health and Medical Research Council of Australia (APP1125794) and The University of Queensland Early Career Researcher.

## Competing Interests

The authors have declared that no competing interest exists.

## References

- Huang P, Rong PF, Jin A, Yan XF, Zhang MG, Lin J, Hu H, Wang Z, Yue XY, Li WW, Niu G, Zeng WB, Wang W, Zhou KC, & Chen XY. Dye-Loaded Ferritin Nanocages for Multimodal Imaging and Photothermal Therapy. *Adv Mater.* 2014; 26: 6401-6408.
- Chen XY, Gambhir SS, & Cheon J. Theranostic Nanomedicine. *Acc Chem Res.* 2011; 44: 841-841.
- Melancon MP, Zhou M, & Li C. Cancer Theranostics with Near-Infrared Light-Activatable Multimodal Nanoparticles. *Acc Chem Res.* 2011; 44: 947-956.
- Jokerst JV & Gambhir SS. Molecular Imaging with Theranostic Nanoparticles. *Acc Chem Res.* 2011; 44: 1050-1060.
- Boni L, David G, Mangano A, Dionigi G, Rausei S, Spampatti S, Cassinotti E, & Fingerhut A. Clinical applications of indocyanine green (ICG) enhanced fluorescence in laparoscopic surgery. *Surg Endosc.* 2015; 29: 2046-2055.
- Sheng ZH, Hu DH, Xue MM, He M, Gong P, & Cai LT. Indocyanine Green Nanoparticles for Theranostic Applications. *Nano-Micro Lett.* 2013; 5: 145-150.
- Wang XD, Ku G, Wegiel MA, Bornhop DJ, Stoica G, & Wang LHV. Noninvasive photoacoustic angiography of animal brains in vivo with near-infrared light and an optical contrast agent. *Opt Lett.* 2004; 29: 730-732.
- Kuo WS, Chang YT, Cho KC, Chiu KC, Lien CH, Yeh CS, & Chen SJ. Gold nanomaterials conjugated with indocyanine green for dual-modality photodynamic and photothermal therapy. *Biomaterials.* 2012; 33: 3270-3278.
- Wang YW, Fu YY, Peng QL, Guo SS, Liu G, Li J, Yang HH, & Chen GN. Dye-enhanced graphene oxide for photothermal therapy and photoacoustic imaging. *J Mater Chem B.* 2013; 1: 5762-5767.
- Yaseen MA, Yu J, Jung BS, Wong MS, & Anvari B. Biodistribution of Encapsulated Indocyanine Green in Healthy Mice. *Mol Pharm.* 2009; 6: 1321-1332.
- Gravier J, Navarro FP, Delmas T, Mittler F, Couffin AC, Vinet F, & Texier I. Lipidots: competitive organic alternative to quantum dots for in vivo fluorescence imaging. *J Biomed Opt.* 2011; 16: 096013.
- Sayag D, Cabon Q, Texier I, Navarro FP, Boisgard R, Virieux-Watrelet D, Carozzo C, & Ponce F. Phase-0/phase-I study of dye-loaded lipid nanoparticles for near-infrared fluorescence imaging in healthy dogs. *Eur J Pharm Biopharm.* 2016; 100: 85-93.
- Merian J, Boisgard R, Bayle PA, Bardet M, Tavitian B, & Texier I. Comparative biodistribution in mice of cyanine dyes loaded in lipid nanoparticles. *Eur J Pharm Biopharm.* 2015; 93: 1-10.
- Zhao PF, Zheng MB, Yue CX, Luo ZY, Gong P, Gao GH, Sheng ZH, Zheng CF, & Cai LT. Improving drug accumulation and photothermal efficacy in tumor depending on size of ICG loaded lipid-polymer nanoparticles. *Biomaterials.* 2014; 35: 6037-6046.
- Beziere N, Lozano N, Nunes A, Salichs J, Queiros D, Kostarelou K, & Ntziachristos V. Dynamic imaging of PEGylated indocyanine green (ICG) liposomes within the tumor microenvironment using multi-spectral optoacoustic tomography (MSOT). *Biomaterials.* 2015; 37: 415-424.
- Bahmani B, Lytle CY, Walker AM, Gupta S, Vullev VI, & Anvari B. Effects of nanoencapsulation and PEGylation on biodistribution of indocyanine green in healthy mice: quantitative fluorescence imaging and analysis of organs. *Int J Nanomedicine.* 2013; 8: 1609-1620.
- Lee CH, Cheng SH, Wang YJ, Chen YC, Chen NT, Souris J, Chen CT, Mou CY, Yang CS, & Lo LW. Near-Infrared Mesoporous Silica Nanoparticles for Optical Imaging: Characterization and In Vivo Biodistribution. *Adv Funct Mater.* 2009; 19: 215-222.
- Souris JS, Lee CH, Cheng SH, Chen CT, Yang CS, Ho JAA, Mou CY, & Lo LW. Surface charge-mediated rapid hepatobiliary excretion of mesoporous silica nanoparticles. *Biomaterials.* 2010; 31: 5564-5574.
- Huang J, Shu Q, Wang LY, Wu H, Wang AY, & Mao H. Layer-by-layer assembled milk protein coated magnetic nanoparticle enabled oral drug delivery with high stability in stomach and enzyme-responsive release in small intestine. *Biomaterials.* 2015; 39: 105-113.
- Ashokan A, Gowd GS, Somasundaram VH, Bhupathi A, Peethambaran R, Unni AKK, Palaniswamy S, Nair SV, & Koyakutty M. Multifunctional calcium phosphate nano-contrast agent for combined nuclear, magnetic and near-infrared in vivo imaging. *Biomaterials.* 2013; 34: 7143-7157.
- Luk BT, Fang RH, & Zhang LF. Lipid- and Polymer-Based Nanostructures for Cancer Theranostics. *Theranostics.* 2012; 2: 1117-1126.
- Slowing II, Trewyn BC, Giri S, & Lin VSY. Mesoporous silica nanoparticles for drug delivery and biosensing applications. *Adv Funct Mater.* 2007; 17: 1225-1236.
- Gupta AK & Gupta M. Synthesis and surface engineering of iron oxide nanoparticles for biomedical applications. *Biomaterials.* 2005; 26: 3995-4021.
- Altinoglu EI, Russin TJ, Kaiser JM, Barth BM, Eklund PC, Kester M, & Adair JH. Near-infrared emitting fluorophore-doped calcium phosphate nanoparticles for in vivo imaging of human breast cancer. *ACS Nano.* 2008; 2: 2075-2084.

25. Yi X, Wang F, Qin W, Yang X, & Yuan J. Near-infrared fluorescent probes in cancer imaging and therapy: an emerging field. *Int J Nanomedicine*. 2014; 9: 1347-1365.
26. Zhang HF, Maslov K, Stoica G, & Wang LV. Functional photoacoustic microscopy for high-resolution and noninvasive in vivo imaging. *Nat Biotechnol*. 2006; 24: 848-851.
27. Siphanto RI, Thumma KK, Kolkman RG, van Leeuwen TG, de Mul FF, van Neck JW, van Adrichem LN, & Steenbergen W. Serial noninvasive photoacoustic imaging of neovascularization in tumor angiogenesis. *Opt Express*. 2005; 13: 89-95.
28. Sevick-Muraca EM. Translation of Near-Infrared Fluorescence Imaging Technologies: Emerging Clinical Applications. *Annu Rev Med*. 2012; 63: 217-231.
29. Morita Y, Sakaguchi T, Unno N, Shibasaki Y, Suzuki A, Fukumoto K, Inaba K, Baba S, Takehara Y, Suzuki S, & Konno H. Detection of hepatocellular carcinomas with near-infrared fluorescence imaging using indocyanine green: its usefulness and limitation. *Int J Clin Oncol*. 2013; 18: 232-241.
30. Schaafsma BE, Mieog JSD, Hutteman M, Van der Vorst JR, Kuppen PJK, Lowik CWGM, Frangioni JV, Van de Velde CJH, & Vahrmeijer AL. The Clinical Use of Indocyanine Green as a Near-Infrared Fluorescent Contrast Agent for Image-Guided Oncologic Surgery. *J Surg Oncol*. 2011; 104: 323-332.
31. Vahrmeijer AL, Hutteman M, van der Vorst JR, van de Velde CJH, & Frangioni JV. Image-guided cancer surgery using near-infrared fluorescence. *Nat Rev Clin Oncol*. 2013; 10: 507-518.
32. Handgraaf HJ, Verbeek FP, Tummers QR, Boogerd LS, van de Velde CJ, Vahrmeijer AL, & Gaarenstroom KN. Real-time near-infrared fluorescence guided surgery in gynecologic oncology: a review of the current state of the art. *Gynecol Oncol*. 2014; 135: 606-613.
33. Gilmore DM, Khullar OV, Gioux S, Stockdale A, Frangioni JV, Colson YL, & Russell SE. Effective low-dose escalation of indocyanine green for near-infrared fluorescent sentinel lymph node mapping in melanoma. *Ann Surg Oncol*. 2013; 20: 2357-2363.
34. Gotoh K, Yamada T, Ishikawa O, Takahashi H, Eguchi H, Yano M, Ohigashi H, Tomita Y, Miyamoto Y, & Imaoka S. A novel image-guided surgery of hepatocellular carcinoma by indocyanine green fluorescence imaging navigation. *J Surg Oncol*. 2009; 100: 75-79.
35. Holt D, Okusanya O, Judy R, Venegas O, Jiang J, DeJesus E, Eruslanov E, Quatromoni J, Bhojnagarwala P, Deshpande C, Albelda S, Nie S, & Singhal S. Intraoperative Near-Infrared Imaging Can Distinguish Cancer from Normal Tissue but Not Inflammation. *Plos One*. 2014; 9: e103342.
36. Saxena V, Sadoqi M, & Shao J. Degradation kinetics of indocyanine green in aqueous solution. *J Pharm Sci*. 2003; 92: 2090-2097.
37. Mordon S, Devoisselle JM, Soulie-Begu S, & Desmettre T. Indocyanine green: physicochemical factors affecting its fluorescence in vivo. *Microvasc Res*. 1998; 55: 146-152.
38. Song S, Shen H, Yang T, Wang L, Fu H, Chen H, & Zhang Z. Indocyanine Green Loaded Magnetic Carbon Nanoparticles for Near Infrared Fluorescence/Magnetic Resonance Dual-Modal Imaging and Photothermal Therapy of Tumor. *ACS Appl Mater Interfaces*. 2017; 9: 9484-9495.
39. Barth BM, Sharma R, Altinoglu EI, Morgan TT, Shanmugavelandy SS, Kaiser JM, McGovern C, Matters GL, Smith JP, Kester M, & Adair JH. Bioconjugation of Calcium Phosphosilicate Composite Nanoparticles for Selective Targeting of Human Breast and Pancreatic Cancers In Vivo. *ACS Nano*. 2010; 4: 1279-1287.
40. Tsuchimochi M, Hayama K, Toyama M, Sasagawa I, & Tsubokawa N. Dual-modality imaging with Tc-99m and fluorescent indocyanine green using surface-modified silica nanoparticles for biopsy of the sentinel lymph node: an animal study. *EJNMMI Res*. 2013; 3: 33.
41. Yamaguchi H, Tsuchimochi M, Hayama K, Kawase T, & Tsubokawa N. Dual-Labeled Near-Infrared/Tc-99m Imaging Probes Using PAMAM-Coated Silica Nanoparticles for the Imaging of HER2-Expressing Cancer Cells. *Int J Mol Sci*. 2016; 17: 1086.
42. Zeng CT, Shang WT, Wang K, Chi CW, Jia XH, Fang C, Yang D, Ye JZ, Fang CH, & Tian J. Intraoperative Identification of Liver Cancer Microfoci Using a Targeted Near-Infrared Fluorescent Probe for Imaging-Guided Surgery. *Sci Rep*. 2016; 6: 21959.
43. Kim TH, Chen YP, Mount CW, Gombotz WR, Li XD, & Pun SH. Evaluation of Temperature-Sensitive, Indocyanine Green-Encapsulating Micelles for Noninvasive Near-Infrared Tumor Imaging. *Pharm Res*. 2010; 27: 1900-1913.
44. Mok H, Jeong H, Kim SJ, & Chung BH. Indocyanine green encapsulated nanogels for hyaluronidase activatable and selective near infrared imaging of tumors and lymph nodes. *Chem Commun (Camb)*. 2012; 48: 8628-8630.
45. Zheng MB, Zhao PF, Luo ZY, Gong P, Zheng CF, Zhang PF, Yue CX, Gao DY, Ma YF, & Cai LT. Robust ICG Theranostic Nanoparticles for Folate Targeted Cancer Imaging and Highly Effective Photothermal Therapy. *ACS Appl Mater Interfaces*. 2014; 6: 6709-6716.
46. Hill TK, Abdulahad A, Kelkar SS, Marini FC, Long TE, Provenzale JM, & Mohs AM. Indocyanine Green-Loaded Nanoparticles for Image-Guided Tumor Surgery. *Bioconjug Chem*. 2015; 26: 294-303.
47. Tsujimoto H, Morimoto Y, Takahata R, Nomura S, Yoshida K, Hiraki S, Horiguchi H, Miyazaki H, Ono S, Saito D, Hara I, Ozeki E, Yamamoto J, & Hase K. Theranostic Photosensitive Nanoparticles for Lymph Node Metastasis of Gastric Cancer. *Ann Surg Oncol*. 2015; 22: S923-S928.
48. Suganami A, Iwadate Y, Shibata S, Yamashita M, Tanaka T, Shinozaki N, Aoki I, Saeki N, Shirasawa H, Okamoto Y, & Tamura Y. Liposomally formulated phospholipid-conjugated indocyanine green for intra-operative brain tumor detection and resection. *Int J Pharm*. 2015; 496: 401-406.
49. Lovell JF, Jin CS, Huynh E, Jin HL, Kim C, Rubinstein JL, Chan WCW, Cao WG, Wang LV, & Zheng G. Porphyosome nanovesicles generated by porphyrin bilayers for use as multimodal biophotonic contrast agents. *Nat Mater*. 2011; 10: 324-332.
50. Zha ZB, Deng ZJ, Li YY, Li CH, Wang JR, Wang SM, Qu EZ, & Dai ZF. Biocompatible polypyrrole nanoparticles as a novel organic photoacoustic contrast agent for deep tissue imaging. *Nanoscale*. 2013; 5: 4462-4467.
51. Ng KK, Shakiba M, Huynh E, Weersink RA, Roxin A, Wilson BC, & Zheng G. Stimuli-responsive photoacoustic nanoswitch for in vivo sensing applications. *ACS Nano*. 2014; 8: 8363-8373.
52. Weber J, Beard PC, & Bohndiek SE. Contrast agents for molecular photoacoustic imaging. *Nat Methods*. 2016; 13: 639-650.
53. Kim C, Song KH, Gao F, & Wang LHV. Sentinel Lymph Nodes and Lymphatic Vessels: Noninvasive Dual-Modality in Vivo Mapping by Using Indocyanine Green in Rats-Volumetric Spectroscopic Photoacoustic Imaging and Planar Fluorescence Imaging. *Radiology*. 2010; 255: 442-450.
54. Landsman ML, Kwant G, Mook GA, & Zijlstra WG. Light-absorbing properties, stability, and spectral stabilization of indocyanine green. *J Appl Physiol*. 1976; 40: 575-583.
55. de la Zerda A, Liu ZA, Bodapati S, Teed R, Vaithilingam S, Khuri-Yakub BT, Chen XY, Dai HJ, & Gambhir SS. Ultrahigh Sensitivity Carbon Nanotube Agents for Photoacoustic Molecular Imaging in Living Mice. *Nano Lett*. 2010; 10: 2168-2172.
56. Gao C, Deng ZJ, Peng D, Jin YS, Ma Y, Li YY, Zhu YK, Xi JZ, Tian J, Dai ZF, Li CH, & Liang XL. Near-infrared dye-loaded magnetic nanoparticles as photoacoustic contrast agent for enhanced tumor imaging. *Cancer Biol Med*. 2016; 13: 349-359.
57. Zhang LW, Gao S, Zhang F, Yang K, Ma QJ, & Zhu L. Activatable Hyaluronic Acid Nanoparticle as a Theranostic Agent for Optical/Photoacoustic Image-Guided Photothermal Therapy. *ACS Nano*. 2014; 8: 12250-12258.
58. Sykes EA, Chen J, Zheng G, & Chan WCW. Investigating the Impact of Nanoparticle Size on Active and Passive Tumor Targeting Efficiency. *ACS Nano*. 2014; 8: 5696-5706.
59. Albanese A, Tang PS, & Chan WCW. The Effect of Nanoparticle Size, Shape, and Surface Chemistry on Biological Systems. *Annu Rev Biomed Eng*. 2012; 14: 1-16.
60. Yue CX, Liu P, Zheng MB, Zhao PF, Wang YQ, Ma YF, & Cai LT. IR-780 dye loaded tumor targeting theranostic nanoparticles for NIR imaging and photothermal therapy. *Biomaterials*. 2013; 34: 6853-6861.
61. Wu M, Wang QT, Zhang D, Liao NS, Wu LJ, Huang AM, & Liu XL. Magnetite nanocluster@poly(dopamine)-PEG@ indocyanine green nanobead with magnetic field-targeting enhanced MR imaging and photothermal therapy in vivo. *Colloids Surf B Biointerfaces*. 2016; 141: 467-475.
62. Zheng XH, Zhou FF, Wu BY, Chen WR, & Xing D. Enhanced Tumor Treatment Using Biofunctional Indocyanine Green-Containing Nanostructure by Intratumoral or Intravenous Injection. *Mol Pharm*. 2012; 9: 514-522.
63. Chen Z, Zhao PF, Luo ZY, Zheng MB, Tian H, Gong P, Gao GH, Pan H, Liu LL, Ma AQ, Cui HD, Ma YF, & Cai LT. Cancer Cell Membrane-Biomimetic Nanoparticles for Homologous-Targeting Dual-Modal Imaging and Photothermal Therapy. *ACS Nano*. 2016; 10: 10049-10057.
64. Song S, Shen H, Yang T, Wang L, Fu H, Chen H, & Zhang Z. Indocyanine Green Loaded Magnetic Carbon Nanoparticles for Near Infrared Fluorescence/Magnetic Resonance Dual-Modal Imaging and Photothermal Therapy of Tumor. *ACS Appl Mater Interfaces*. 2017; 7: 18557.
65. Cai W, Gao HY, Chu CC, Wang XY, Wang JQ, Zhang PF, Lin G, Li WG, Liu G, & Chen XY. Engineering Phototheranostic Nanoscale Metal-Organic Frameworks for Multimodal Imaging-Guided Cancer Therapy. *ACS Appl Mater Interfaces*. 2017; 9: 2040-2051.
66. Hiscox S, Barua B, Smith C, Bellerby R, Goddard L, Jordan N, Poghosyan Z, Nicholson RI, Barrett-Lee P, & Gee J. Overexpression of CD44 accompanies acquired tamoxifen resistance in MCF7 cells and augments their sensitivity to the stromal factors, heregulin and hyaluronan. *BMC Cancer*. 2012; 12: 458.
67. Wang X, Li J, Wang YQ, Cho KJ, Kim G, Gjyzezi A, Koenig L, Giannakakou P, Shin HJC, Tighiouart M, Nie SM, Chen Z, & Shin DM. HFT-T, a Targeting Nanoparticle, Enhances Specific Delivery of Paclitaxel to Folate Receptor-Positive Tumors. *ACS Nano*. 2009; 3: 3165-3174.
68. Ma Y, Tong S, Bao G, Gao C, & Dai ZF. Indocyanine green loaded SPIO nanoparticles with phospholipid-PEG coating for dual-modal imaging and photothermal therapy. *Biomaterials*. 2013; 34: 7706-7714.
69. Perrault SD, Walkey C, Jennings T, Fischer HC, & Chan WCW. Mediating Tumor Targeting Efficiency of Nanoparticles Through Design. *Nano Lett*. 2009; 9: 1909-1915.
70. Oleinick NL, Morris RL, & Belichenko T. The role of apoptosis in response to photodynamic therapy: what, where, why, and how. *Photochem Photobiol Sci*. 2002; 1: 1-21.
71. Ortner MA. Photodynamic therapy for cholangiocarcinoma: overview and new developments. *Curr Opin Gastroenterol*. 2009; 25: 472-476.
72. Skrivanova K, Skorpikova J, Svihalek J, Mornstein V, & Janisch R. Photophysical properties of a potential photosensitizer indocyanine green in vitro. *J Photochem Photobiol B*. 2006; 85: 150-154.
73. Tsujimoto H, Morimoto Y, Takahata R, Nomura S, Yoshida K, Horiguchi H, Hiraki S, Ono S, Miyazaki H, Saito D, Hara I, Ozeki E, Yamamoto J, & Hase K. Photodynamic therapy using nanoparticle loaded with indocyanine green for

- experimental peritoneal dissemination of gastric cancer. *Cancer Sci.* 2014; 105: 1626-1630.
74. Luo ZY, Zheng MB, Zhao PF, Chen Z, Siu FM, Gong P, Gao GH, Sheng ZH, Zheng CF, Ma YF, & Cai LT. Self-Monitoring Artificial Red Cells with Sufficient Oxygen Supply for Enhanced Photodynamic Therapy. *Sci Rep.* 2016; 6: 3393.
75. Master A, Livingston M, & Sen Gupta A. Photodynamic nanomedicine in the treatment of solid tumors: Perspectives and challenges. *J Control Release.* 2013; 168: 88-102.
76. Reddy GR, Bhojani MS, McConville P, Moody J, Moffat BA, Hall DE, Kim G, Koo YEL, Woolliscroft MJ, Sugai JV, Johnson TD, Philbert MA, Kopelman R, Rehemtulla A, & Ross BD. Vascular targeted nanoparticles for imaging and treatment of brain tumors. *Clin Cancer Res.* 2006; 12: 6677-6686.
77. Barth BM, Altinoglu EI, Shanmugavelandy SS, Kaiser JM, Crespo-Gonzalez D, DiVittore NA, McGovern C, Goff TM, Keasey NR, Adair JH, Loughran TP, Claxton DF, & Kester M. Targeted Indocyanine-Green-Loaded Calcium Phosphosilicate Nanoparticles for In Vivo Photodynamic Therapy of Leukemia. *ACS Nano.* 2011; 5: 5325-5337.
78. Zheng XH, Xing D, Zhou FF, Wu BY, & Chen WR. Indocyanine Green-Containing Nanostructure as Near Infrared Dual-Functional Targeting Probes for Optical Imaging and Photothermal Therapy. *Mol Pharm.* 2011; 8: 447-456.
79. Zhong JP, Yang SH, Zheng XH, Zhou T, & Xing D. In vivo photoacoustic therapy with cancer-targeted indocyanine green-containing nanoparticles. *Nanomedicine (Lond).* 2013; 8: 903-919.
80. Sheng ZH, Hu DH, Zheng MB, Zhao PF, Liu HL, Gao DY, Gong P, Gao GH, Zhang PF, Ma YF, & Cai LT. Smart Human Serum Albumin-Indocyanine Green Nanoparticles Generated by Programmed Assembly for Dual-Modal Imaging-Guided Cancer Synergistic Phototherapy. *ACS Nano.* 2014; 8: 12310-12322.
81. You Q, Sun Q, Wang J, Tan X, Pang X, Liu L, Yu M, Tan F, & Li N. A single-light triggered and dual-imaging guided multifunctional platform for combined photothermal and photodynamic therapy based on TD-controlled and ICG-loaded CuS@mSiO<sub>2</sub>. *Nanoscale.* 2017; 9: 3784-3796.
82. Yan F, Wu H, Liu HM, Deng ZT, Liu H, Duan WL, Liu X, & Zheng HR. Molecular imaging-guided photothermal/photodynamic therapy against tumor by iRGD-modified indocyanine green nanoparticles. *J Control Release.* 2016; 224: 217-228.
83. Wang K, Zhang XF, Liu Y, Liu C, Jiang BH, & Jiang YY. Tumor penetrability and anti-angiogenesis using iRGD-mediated delivery of doxorubicin-polymer conjugates. *Biomaterials.* 2014; 35: 8735-8747.
84. Scaringi C, Enrici RM, & Minniti G. Combining molecular targeted agents with radiation therapy for malignant gliomas. *Onco Targets Ther.* 2013; 6: 1079-1095.
85. Peer D, Karp JM, Hong S, Farokhzad OC, Margalit R, & Langer R. Nanocarriers as an emerging platform for cancer therapy. *Nat Nanotechnol.* 2007; 2: 751-760.
86. Hao YW, Wang L, Zhao YL, Meng DH, Li D, Li HX, Zhang BX, Shi JJ, Zhang HL, Zhang ZZ, & Zhang Y. Targeted Imaging and Chemo-Phototherapy of Brain Cancer by a Multifunctional Drug Delivery System. *Macromol Biosci.* 2015; 15: 1571-1585.
87. Zheng MB, Yue CX, Ma YF, Gong P, Zhao PF, Zheng CF, Sheng ZH, Zhang PF, Wang ZH, & Cai LT. Single-Step Assembly of DOX/ICG Loaded Lipid-Polymer Nanoparticles for Highly Effective Chemo-photothermal Combination Therapy. *ACS Nano.* 2013; 7: 2056-2067.
88. Hogset A, Prasmickaite L, Selbo PK, Hellum M, Engesaeter BO, Bonsted A, & Berg K. Photochemical internalisation in drug and gene delivery. *Adv Drug Deliv Rev.* 2004; 56: 95-115.
89. Zhao PF, Zheng MB, Luo ZY, Gong P, Gao GH, Sheng ZH, Zheng CF, Ma YF, & Cai LT. NIR-driven Smart Theranostic Nanomedicine for On-demand Drug Release and Synergistic Antitumour Therapy. *Sci Rep.* 2015; 5: 14258.
90. Zhang EL, Luo SL, Tan X, & Shi CM. Mechanistic study of IR-780 dye as a potential tumor targeting and drug delivery agent. *Biomaterials.* 2014; 35: 771-778.
91. Zheng CF, Zheng MB, Gong P, Jia DX, Zhang PF, Shi BH, Sheng ZH, Ma YF, & Cai LT. Indocyanine green-loaded biodegradable tumor targeting nanoprobe for in vitro and in vivo imaging. *Biomaterials.* 2012; 33: 5603-5609.